

# Comparison of near-surface properties derived from non-linear inversion of refraction amplitudes versus the refraction convolution section

**Alan Meulenbroek**

*Velseis Pty Ltd and School of Earth Sciences, University of Queensland  
 PO Box 118, Sumner Park,  
 Queensland, Australia 4074  
 alanm@velseis.com*

## SUMMARY

The amplitude of a seismic refraction event is dependent on the properties of the rocks through which the seismic waves travel, the amplitude of the shot, and the offset at which the refraction is recorded. Separation and subsequent analysis of these 3 constituent amplitude terms can provide insight into the physical properties of the near-surface. A comparison between a published method of amplitude separation and a formal, non-linear, inversion scheme is presented using a Vibroseis dataset as the test case.

An assessment of the two methods shows that there is very good correlation for this dataset. Variations in the curves representing lateral changes in physical properties are consistent with each other along most of the extent of the line. The range of values for the non-linear inversion result is consistent with theoretical values for most near-surface geologies.

**Key words:** Seismic refraction, inversion, amplitude, near-surface.

## INTRODUCTION

The definition of the near-surface can vary depending on the context in which the term is used. In a seismic reflection survey, the near-surface is generally considered to consist of the weathering layer and the interface between the weathering and the sub-weathering layers (the base of weathering). Understanding the properties of this region is important because corrections must be made in order to account for variations in near-surface properties. In a seismic reflection survey, the study of these near-surface properties is generally restricted to variations in arrival times of critically refracted waves. The corresponding amplitudes are typically ignored.

In reflection seismology, the amplitude of a seismic event can provide additional information useful to the characterisation of the deep sub-surface (AVO). Similarly, the analysis of the amplitude of a seismic refraction event can yield additional information useful in the characterisation of the near-surface.

The amplitude of a seismic refraction is proportional to the magnitude of the shot and inversely on the offset at which the event is measured. The constant of proportionality is called the head-wave coefficient. This head-wave coefficient is a complex function of the elastic properties through which the critically refracted wave propagates (Červený and Ravindra, 1971). With proper analysis it may be feasible to derive a

near-surface velocity profile useful in refraction statics and geotechnical investigations.

There have been many derivations of the head-wave coefficient published using various methods (e.g. Heelan, 1953; Zvolinskii, 1958, Červený and Ravindra, 1971). However, very few authors have published methods of obtaining the head-wave coefficient from refraction amplitudes in an attempt to derive the causative elastic properties of the near-surface. In order to measure the head-wave coefficient, the constituent shot and offset dependence must be removed from the measured refraction amplitude. Palmer (2001a, 2001b) published a method of doing this called the refraction convolution section (RCS). Meulenbroek (2010) presented an alternative technique where the problem is formulated as a formal, non-linear inverse problem.

This paper presents a comparison of the two methods on a Vibroseis-scale dataset acquired for the Australian National Seismic Imaging Resource (ANSIR) in 1999.

## BACKGROUND THEORY

With reference to Figure 1, Equation 1 shows the expression for the refraction amplitude originating from a source,  $S$ , with a magnitude,  $F(t)$ , recorded by a geophone,  $G$ , which is at an offset,  $r$  from  $S$ .

$$\text{Amplitude} = \frac{KF(t)}{(rL^3)^{1/2}} \quad (1)$$

The distance the wave travels in the refractor,  $L$ , depends on the depth to the refractor,  $z$ , and the critical angle of refraction,  $i_c$ .

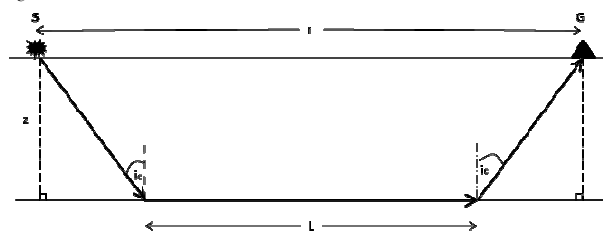


**Figure 1: Ray-path diagram of critically refracted wave originating from the source,  $S$ , and recorded by a geophone,  $G$ , at an offset,  $r$ .**

In order to deduce  $K$  (which is a function of the near-surface elastic properties), it must be separated from the shot and offset terms. Palmer (2001a, 2001b) presents a method of separation which involves the convolution of traces at a common receiver location between two shots, one of which is in front of the common receiver, the other of which is behind the common receiver. In this technique, the offset terms are mitigated sufficiently to facilitate analysis of the receiver

terms of interest. Individual RCS pairs are then stacked based on receiver location to increase the signal to noise ratio, and amplitude interpretation is possible from the final stacked section. The amplitude of the first event on the RCS is proportional to the square of the head-wave coefficient ( $K^2$ ). This is because the amplitude spectra of the two traces have been multiplied in the convolution process. Variations in amplitude along the line can then be attributed to near-surface property (e.g. density, velocity) changes.

A completely different method of separating the shot, receiver and offset dependence is to formulate the problem as an overdetermined system of equations, analogous to the residual statics algorithm. Each individual refraction amplitude measurement (measured at each receiver) originates from a unique combination of model parameters. These model parameters are the shot term ( $F(i)$ ), the receiver term ( $K$ ) and the offset term (denominator in Equation 1). This can be expressed as a system of equations of the form:

$$\mathbf{Ax} = \mathbf{b} \quad (2)$$

where  $\mathbf{x}$  is the  $N$  vector of model parameter;  $\mathbf{b}$  is the  $M$  vector of observations and  $\mathbf{A}$  is the binary  $M \times N$  matrix relating each observation to the model parameters. This system of equations has  $M$  equations in  $N$  unknowns. Because  $M > N$ , the system is overdetermined and can be solved using the least-squares criterion. However, because the observations are a non-linear combination of model parameters (Equation 1), the system is non-linear and cannot be solved using simple linear least-squares inversion techniques (such as those used for residual statics). The nonlinear problem is given by:

$$b_i = \prod_{j=1}^n (A_{ij} x_j) \quad (i=1, m) \quad (3)$$

The algorithm used to solve this nonlinear problem is the Levenberg-Marquardt algorithm. For this study, a widely used implementation of the algorithm, namely the PEST suite of programs (Doherty, 2004, 2010), is used. In the following, the PEST terminology is broadly used, although the comments are applicable to non-linear inversion algorithms in general.

## PRACTICAL CONSIDERATIONS

It is very important that any inversion scheme be targeted specifically to the problem in question. This includes, but is not limited to, adjusting key control parameters which dictate the initial conditions of the problem, how the problem is allowed to progress over time and when the problem is deemed to be optimised.

Regularisation, which can take the form of the application of a-priori information for the purposes of constraining the model parameters, or controlling the ability to handle instabilities in the problem, is critical in determining whether a problem will converge to a solution or not. Hence regularisation is a critical step to creating a well-posed problem.

It is also necessary to consider the relative confidence levels between estimated model parameters. Each model parameter is not equally sampled by the same number of observations. Model parameters which have been estimated with only a few observations are not constrained as well as those parameters which contribute to a large number of observations.

## Solution Appraisal

A post-inversion analysis is required to test whether the problem has been effectively optimised or not. The most common tool is the sum of the squares of the errors between the true observations ( $\mathbf{b\_true}$ ) and the model predicted observations ( $\mathbf{b\_pre}$ ). This is called the objective function ( $\Phi$ ):

$$\phi = \sum_{i=1}^M (b\_true_i - b\_pre_i)^2 \quad (4)$$

In practice, the size of this objective function depends on the scale of the problem in question. This can be an issue when interpreting how well the model predicted observations fit the true observations for models on different scales. The error for a large scale problem may appear to be very large when compared to a small scale problem when in fact, the opposite may be true. To overcome this issue, the concept of the filter performance parameter, FPP, (Robinson and Treitel, 1980) can be used to normalise the errors such that different problems can be compared using the same parameter, regardless of scale. The FPP is defined as 1 minus the ratio of the sum of the squares of the errors to the sum of the squares of the true observations (Equation 5). Subtracting the ratio from 1 creates an intuitive measure of the error in a problem, i.e. the smaller the error, the closer to unity the FPP will be.

$$FPP = 1.0 - \frac{\Phi}{\sum_i^m b\_true_i^2} \quad (5)$$

## REAL DATA EXAMPLE

The real data used in this paper were acquired for ANSIR on behalf of (then) AGSO, AGCRC and NSWDMR in 1999. It is a Vibroseis dataset consisting of a total of 1313 shots, 1697 receivers with 240 live channels (120-0-120 split spread). The group interval is 10m. The line is a combination of half and full fold, i.e. VP interval varies between 10m/20m. This dataset has been chosen because it is the same dataset used by Palmer in various publications (e.g. Palmer, 2009). Direct comparisons can therefore be made between the two methods.

The total number of refraction amplitude observations ( $M$ ) for the full survey is 304555 (by comparison, the total number of traces in the survey is 315120) and the total number of model parameters ( $N$ ) is 3250 (1313 shots, 1697 receivers, 240 offsets). The matrix  $A$  has a total of  $9.89 \times 10^8$  elements, most of which are zero.

For computational reasons, this problem has been split up into 4 separate regions. Breaking a model up into many regions is not ideal because the overlap between regions must be dealt with appropriately. However, analysis of the overlapping regions can also provide independent verification of the consistency of the estimated model parameters.

The near-offset refraction amplitudes have also been eliminated for two reasons. The first is that because there is a variation of depth and seismic velocities along the line, near-offset amplitudes may not actually arise from the critically refracted wave. The inclusion of these data as part of the observations will add noise to the system and inhibit optimisation progress. The second reason is that because the magnitude of the near-offset amplitudes are so high relative to far offset amplitudes, in many cases by up to 5 orders of magnitude, they will tend to dominate the calculation of  $\Phi$ ,

thus inhibiting the optimisation process (Doherty, 2010). Therefore, only offsets greater than 100m have been used in the inversion process. This reduces the total number of observations to 278375. Table 1 (at the end of paper) shows the number of model parameters for each region.

The initial model used for these inversions is the cube-root of the mean of the true observations. This choice of initial model assumes that each model parameter contributes equally to each observation, which, in the absence of any other information, is a valid assumption.

Figure 2 shows the estimated model parameters for the first region (shots 1076-1500). The vertical lines separate the shot, receiver and offset domains. Note the dominant offset term. Although the estimated offset amplitudes are relatively large compared to the shot and offset domains, they are relatively small compared to an inversion which includes the near-offset terms. It is the receiver terms from Figure 2 which are analogous to the amplitude product derived from the RCS. However, in their current form, the receiver terms in Figure 2 are too noisy to glean any information. The application of a smoothing operator eliminates high-frequency noise which enables the underlying, large-scale, structure to be analysed.

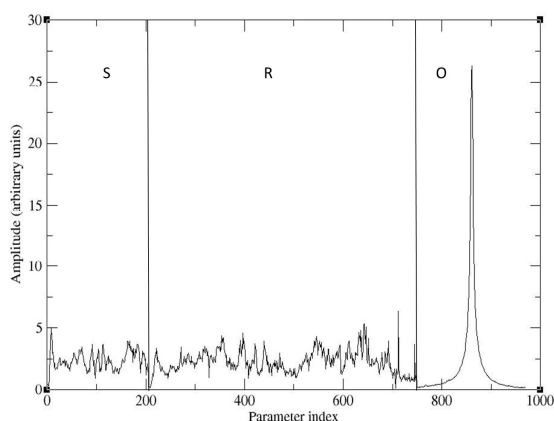


**Figure 2. Estimated model parameters for shot locations 1076-1500. The vertical lines separate the shot (S), receiver (R) and offset (O) domains.**

Figures 3 to 6 show comparisons between the smoothed RCS solution (red; data supplied by Dr Derecke Palmer) and the smoothed inverted solution (black). Note that for display and comparison purposes, the inverted solution has been scaled and shifted vertically using the range and average of the RCS solution. This enables a direct comparison, on the same scale, between the lateral variations in the two solutions.

Overall, there is very good correlation between the locations of the peaks and troughs between the two solutions. There are areas where the two solutions do diverge slightly, most noticeably between stations 1076-1200 on Figure 3. The estimated model parameters in this area are not as well constrained because there are fewer amplitude observations at the start of the spread. This does not seem to be the case at the other end of the line however (Figure 6).

The amplitudes of the two solutions also differ in some areas. This is not entirely unexpected. Because the inverse problem is overdetermined, the solution is not exact. In generating the RCS, a degree of averaging is taking place so the lateral

resolution will also not be precise. This means that an exact correlation between the two will never be achievable. However, the high degree of overall correlation between the two solutions does suggest that both methods are detecting real lateral variations in near-surface physical properties. In general, a higher K is representative of a lower P-wave velocity contrast between the weathering and sub-weathering layers. Conversely, a lower K is representative of a higher P-wave velocity contrast between the weathering and sub-weathering layers.

Table 2 shows the FPPs of the inverted solutions for offsets greater than 100m and for all offsets. With the exception of Region 1, the elimination of very large, near-offset, amplitudes has considerably increased the overall confidence in the solutions. This illustrates how important regularisation of the inverse problem is to achieving a realistic solution, both mathematically and geologically.

	1	2	3	4
<b>Offset &gt;100m</b>	0.901	0.928	0.906	0.905
<b>All offsets</b>	0.927	0.677	0.783	0.477

**Table 2. Filter performance parameters (FPPs) for inversions using different offset ranges.**

### CONCLUSIONS

The consistency between the structure of the two solutions is generally convincing. Both methods, although completely different in their algorithms, have generated the same result in terms of lateral variations of near-surface physical properties.

Analysis of the FPPs shows that regularisation of the problem is critical in obtaining a realistic solution.

Current and future research is focussing on the effect of different methods of reducing the effect that the large amplitude variation with offset has on the resulting estimated model parameters. Methods include subtracting the average of each amplitude at each offset prior to inversion, and log-transforming the data into a linear problem where even the largest amplitude differences are only a single order of magnitude apart.

Once an optimum regularisation regime has been determined, the relationship between the results and the causative geology can be established.

### ACKNOWLEDGMENTS

The real data presented in this paper have been made available by Geoscience Australia. The author also thanks Dr. John Doherty, the author of PEST, for his insight and ongoing consultation. Thanks also to Dr. Derecke Palmer of UNSW for providing results with which to compare the two methods. This research has been, in part, supported by the ASEG research foundation.

### REFERENCES

Červený, V., Ravindra, R., 1971, Theory of seismic head waves, Toronto, university of Toronto Press.

Doherty, J., 2004, PEST – Model-Independent Parameter Estimation User Manual: 5<sup>th</sup> edition, Watermark Numerical Computing.

Doherty, J., 2010, Addendum to the PEST Manual, Watermark Numerical Computing.

Heelan, 1953, On the theory of head waves. *Geophysics*, **18**, pp871-893.

Meulenbroek, A., 2010, Least-squares inversion of refraction amplitudes for near-surface velocity control, Extended Abstracts, ASEG 21<sup>st</sup> International Conference and Exhibition, Sydney.

Palmer, D., 2001a, Imaging refractors with the convolution section, *Geophysics*, **66**, 5, pp1582-1589.

Palmer, D., 2001b, Resolving refractor ambiguities with amplitudes, *Geophysics*, **66**, 5, pp1590-1593.

Palmer, D., 2009, Integrating long and short wavelength time and amplitude statics, *First Break*, **27**, pp57-65.

Robinson, E.A., Treitel, S., 1980, *Geophysical signal analysis*, Prentice Hall International, Inc., London.

Zvolinskii, 1958, Reflected-waves and head-waves arising at a plane interface between two elastic media – II: *Bulletin of the Academy of Sciences of the U.S.S.R. Geophysics Series*), **11**, pp1-7.

	1	2	3	4
<b>Shot range</b>	1076-1500	1501-2000	2001-2400	2401-2772
<b>Receiver range</b>	1076-1619	1382-2119	1881-2519	2281-2772
<b># shots</b>	205	361	385	362
<b># receivers</b>	544	738	639	492
<b># offsets</b>	220	220	220	220
<b># unknowns (N)</b>	969	1319	1244	1074
<b># observations (M)</b>	41623	79420	84700	72632

Table 1. Model parameter ranges for each of the 4 inversion regions for offsets greater than 100m.

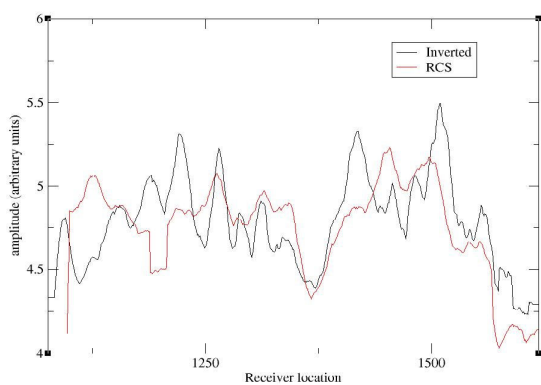


Figure 3. Smoothed inverted (black) vs RCS (red) estimated receiver model parameters, shots 1076-1500.

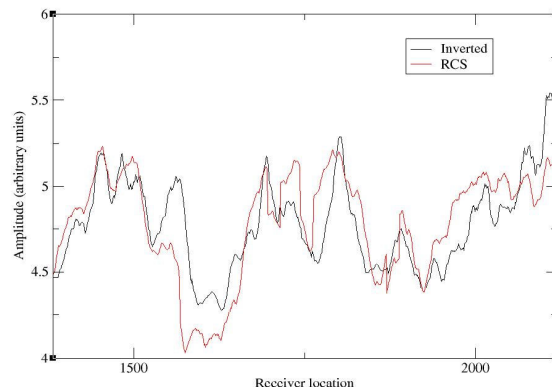


Figure 4. Smoothed inverted (black) vs RCS (red) estimated receiver model parameters, shots 1501-2000.

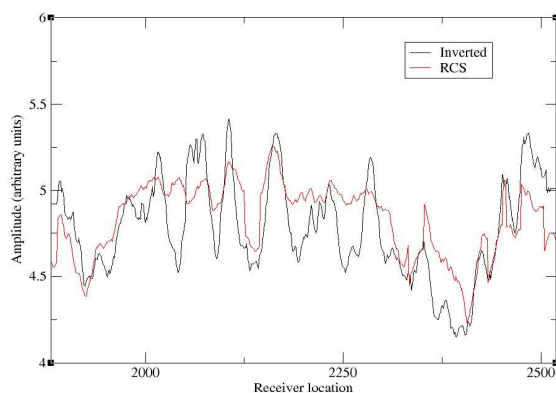


Figure 5. Smoothed inverted (black) vs RCS (red) estimated receiver model parameters, shots 2001-2400.

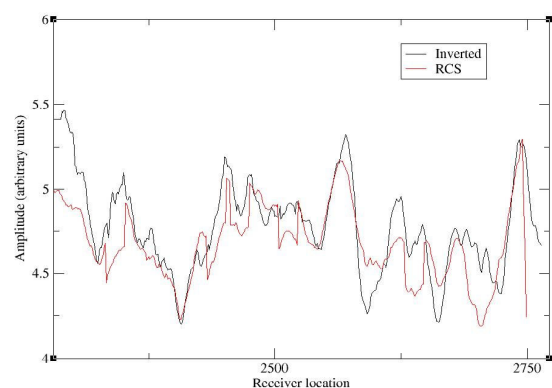


Figure 6. Smoothed inverted (black) vs RCS (red) estimated receiver model parameters, shots 2401-2772.